Research Article | Vol. 29, No. 5 / 1 March 2021 / Optics Express 7601
Optics EXPRESS

Monolithic integration of microlenses on the backside of a silicon photonics chip for expanded beam coupling

NIVESH MANGAL,[1,2] BRADLEY SNYDER,[2] JORIS VAN CAMPENHOUT,[2] GEERT VAN STEENBERGE,[1] AND JEROEN MISSINNE[1,*]

[1] *Centre for Microsystems Technology, Ghent University—imec, Technologiepark-Zwijnaarde 126, 9052 Ghent, Belgium*
[2] *imec, Kapeldreef 75, Heverlee B- 3001, Belgium*
[*] *jeroen.missinne@ugent.be*

Abstract: To increase the manufacturing throughput and lower the cost of silicon photonics packaging, an alignment tolerant approach is required to simplify the process of fiber-to-chip coupling. Here, we demonstrate an alignment-tolerant expanded beam backside coupling interface (in the O-band) for silicon photonics by monolithically integrating microlenses on the backside of the chip. After expanding the diffracted optical beam from a TE-mode grating through the bulk silicon substrate, the beam is collimated with the aid of microlenses resulting in an increased coupling tolerance to lateral and longitudinal misalignment. With an expanded beam diameter of 32 μm, a ±7 μm lateral and a ±0.6° angular fiber-to-microlens 1-dB alignment tolerance is demonstrated at the wavelength of 1310 nm. Also, a large 300 μm longitudinal alignment tolerance with a 0.2 dB drop in coupling efficiency is obtained when the collimated beam from the microlens is coupled into a thermally expanded core single-mode fiber.

1. Introduction

Silicon photonics technology provides integrated die-level optical functionalities with advantages such as single-mode transmission, wavelength division multiplexing and compatibility with established CMOS-manufacturing facilities, leveraging advanced 3D integration schemes to meet high bandwidth demands with low power dissipation [1–3]. This has led to its widespread adoption across several domains such as high-speed optical transceivers [4,5], beam-steering for lidar applications [6,7], metamaterial devices [8,9], mid-infrared sensing [10,11], microwave photonics [12,13], nonlinear optics [14,15], quantum computing [16,17], deep learning [18–20], and neuromorphic networks [21,22]. Optical coupling to silicon photonics chips is performed mostly either by attaching a fiber (with or without incorporating a lens) to an edge coupler or a grating coupler [23]. Due to the submicrometer dimensions of on-chip waveguides (e.g., 0.45 × 0.22 μm^2), coupling light from the external world is not straightforward and poses a serious challenge. Due to that, highly precise alignment accuracies are needed to ensure optimal coupling efficiency. For example, an optical beam when coupled out of a standard grating coupler, that is usually mode-matched to a standard single mode fiber (9.2 μm mode-field diameter at λ = 1310 nm), at best, provides a ±2.5 μm lateral alignment tolerance and necessitates an active alignment driven fiber-array packaging [24]. For a high volume production, this process is time consuming and affects the overall throughput, thereby making the photonics packaging process one of the leading contributing factors to the overall cost of a silicon photonics based functional module [25–27].

Thus, robust passive alignment based strategies are needed that can be low-cost, scalable, generic to any material platform, and are mass deployable. This can be realized by expanding

#412353 https://doi.org/10.1364/OE.412353
Journal © 2021 Received 13 Oct 2020; revised 15 Jan 2021; accepted 26 Jan 2021; published 25 Feb 2021

Optics EXPRESS

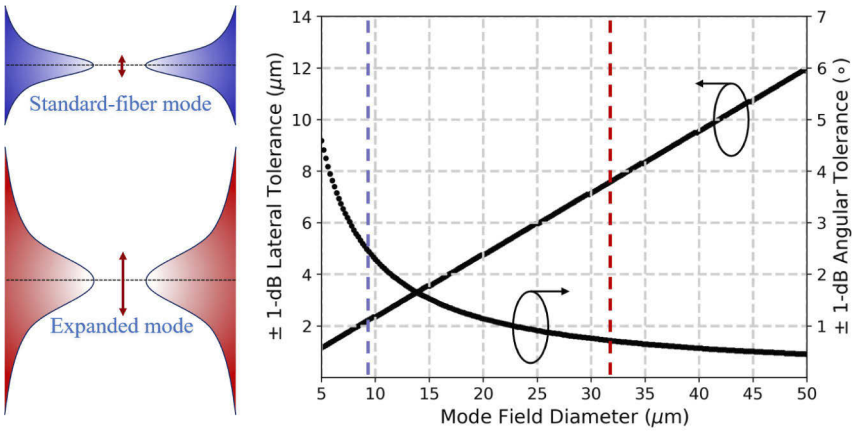

Fig. 1. (a) An expanded mode provides improvement in lateral alignment tolerance in comparison to a standard fiber-like mode. (b) The graph shows the scaling of ±1-dB lateral and angular alignment tolerances with the expansion of beam (Gaussian) diameter (calculations performed using analytical relations in [28]).

the optical beam from the coupling interface to realize a relaxed fiber-to-chip lateral alignment tolerance. As an example, one can obtain a 3x improvement in the lateral alignment tolerance with an expanded mode diameter of 32 μm when compared to a standard fiber mode diameter of 9.2 μm at 1310 nm wavelength (Fig. 1). Although this results in an increased sensitivity to angular misalignment, it can be controlled with the use of an appropriate mechanical design during assembly as long as it is better than 0.1°-limit [29]. Moreover, for beam diameters increasing between 25-50 μm, while the gain in 1-dB lateral alignment tolerance occurs by ±6 μm, the 1-dB angular alignment tolerance shrinks by only ±0.5°. Thus, the penalty incurred to the angular alignment tolerance is not so high compared to the improvements obtained in the lateral alignment tolerance for expanded mode field diameters above 25 μm.

Several efforts have been made in the recent past utilizing V-grooves [25], inverted tapers and sub-wavelength metamaterial mode converters [30,31], forked couplers [32] and 3D-printed optics [33] to relax the alignment margins needed for passive assembly [26,34]. In addition, chip-surface out-of-plane beam expansion and collimation from grating couplers has been a subject of great interest recently. In this direction, a demonstration was made by coupling between a glass-based lens integrated fiber array and microlens hybrid-integrated on the "topside" of a standard grating coupler to result in a ±30 μm 1-dB lateral alignment tolerance [35]. In comparison, efficient "backside" (through-substrate) coupling demonstrations using grating couplers (with metal reflectors) hybrid integrated with backside microlenses fabricated in polymer [36] and silicon [37] have been reported by ourselves in the past, showcasing a fiber-to-grating 1-dB lateral alignment tolerance of ±12 μm and ±7 μm respectively. A backside coupling interface not only avoids the necessity to reserve space for interfacing of a fiber array on the topside of the die but also avoids increasing the thickness of the whole assembly. Furthermore, it offers an alternate route to guide the resultant optical output other than in the conventional device-side direction. This aspect can be utilized for applications such as sensing where the device topside can be kept clear, enabling the interaction between a photonic circuit and biomarkers or trace gas molecules and the optical readout performed using a lensed fiber array from the backside of the chip [38]. Similarly, for co-packaged solutions in datacenters, a face-up bonding scheme of the photonics die is desirable from the perspective of 3D electrical integration of the memory/logic driver chips on the top of

Optics EXPRESS

a photonics chip interposer [39]. A backside coupling interface in this scenario allows a high density optical I/O for high speed transfer of data across the server backplanes [40,41].

An initial demonstration of a monolithic backside coupling interface was showcased recently [38], but it was targeted towards the wavelength range of C-band and a system-level analysis was not performed at that time. Also, the discussion in our earlier work was only limited to the alignment tolerant aspect of the concept, but did not provide the coupling analysis in greater detail. Moreover, the fiber-to-fiber coupling results presented in our previous work were obtained by using a multimode fiber as the output fiber. In comparison, in this paper, we provide a complete single-mode fiber-to-fiber coupling analysis for a target wavelength range in O-band, and investigate the individual contributions in coupling loss of an expanded beam interface. Based on these results, we provide suggestions for future improvements and project the net reduction in overall loss that can be achieved in a monolithically fabricated expanded beam interface. Also, in comparison to our previous work on Si microlenses using hybrid integration [37], this paper discusses the generic design challenges in greater detail incorporating all the parametric degrees of freedom in the design space, when implementing expanded beam coupling interfaces for integrated photonics chips for any wavelength range and material platform. Separately, both top-side and back-side coupling and testing strategies are explored to arrive at an optimum coupling performance of the expanded beam interface. This also generates different application-dependent integration possibilities for a designer targeting to implement the concept. Lastly, by integrating microlenses monolithically, the paper demonstrates the potential of extending this concept at wafer-scale for alignment-tolerant optics across different material platforms.

2. Generic concept and design principles to realize An expanded beam coupling interface

The concept of expanded beam collimation in itself is very generic, and can be implemented for other wavelength bands and material platforms for integrated optics (e.g. SiN, InP etc.), as long as the substrate material is transparent to a corresponding wavelength range. The operating principle of expanded beam collimation using a photonics chip integrated with backside microlenses is as follows: the photonics chip consists of downward directionality based grating couplers that diffract the incoming optical waveguide mode at an angle into the bulk silicon substrate. The diffracted beam expands in the silicon substrate and is collimated with the help of a microlens with a particular radius of curvature. The expanded and collimated optical beam from the backside microlens is then coupled into a thermally expanded-core (TEC) fiber with a similar mode-field diameter (Fig. 2). The enlarged mode field diameter of a thermally expanded core

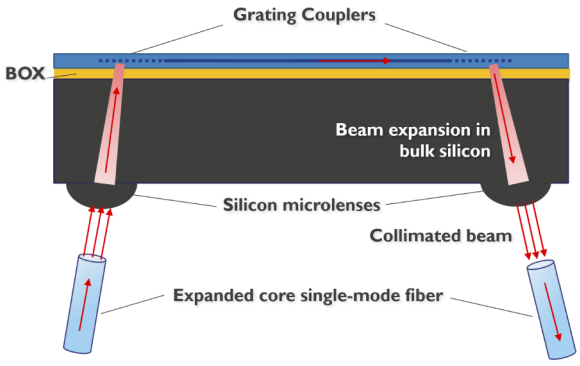

Fig. 2. An overview of photonics chip expanded-beam coupling interface.

Optics EXPRESS

(TEC) fiber is obtained by locally heating a single-mode fiber at high temperature resulting in the redistribution of dopants while maintaining the single-mode condition of the fiber [42,43]. As an alternative, a fiber-lens assembly optimized for a collimated beam of a particular diameter can also be used to perform coupling. The results presented here, however have been achieved with the commercially available TEC fibers. To realize such an expanded beam interface, there are some design parameters and boundary conditions (Fig. 3) that need to be evaluated based on the desired final metrics such as final beam diameter, 1-dB lateral and angular alignment tolerance, wavelength range of operation, coupling efficiency etc.

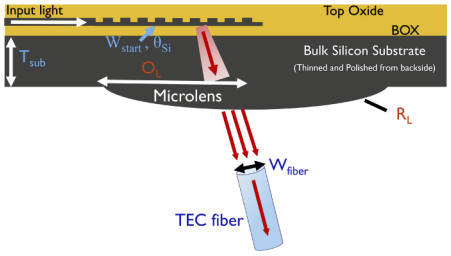

(a)

	Design Boundary Conditions	Parameters
(i)	Starting mode-field diameter	W_{start}
(ii)	Thickness of the substrate	T_{sub}
(iii)	Angle of the beam in Si	θ_{Si}
(iv)	Lens offset from the coupling position of the grating	O_L
(v)	Radius of curvature of the microlens	R_L
(vi)	Fiber (TEC40) mode-field diameter	W_{fiber}

(b)

Fig. 3. (a) A schematic of the expanded beam coupling concept using backside emitting grating couplers, highlighting the parameters available for design and (b) tabulated with the description of those parameters.

(i) Starting mode-field diameter, W_{start}: The mode-field diameter of the optical beam diffracted by the output grating coupler is a critical parameter to determine the final expanded beam diameter, which also depends on the propagation distance (as described in (ii)) and refractive index of the silicon substrate. Besides the mode-field diameter, the field profile emitted from the grating dictates the overall transformation of the beam as it propagates down the substrate and impacts the coupling performance eventually. Thus, an appropriate grating design is required to accomplish the desired metrics.

(ii) Thickness of the substrate, T_{sub}: The propagation distance of the diffracted beam between the grating and the microlens is determined by $T_{sub}/\cos(\theta_{Si})$, where θ_{Si} is the angle of the diffracted beam with respect to normal in the silicon substrate. Thus, various values of expanded beam diameters can be obtained by a conscious choice of substrate thickness and a starting beam diameter at the grating coupler. Assuming Gaussian beam propagation with an initial waist of 4.6 μm (diameter - 9.2 μm) from the designed grating coupler, at an O-band primary wavelength of λ = 1310 nm, the resulting beam diameters (at the microlens) as a function of silicon substrate thickness have been listed in Table 1.

(iii) Angle of the beam in Silicon, θ_{Si}: This parameter is related to the period of the designed grating and determines the resultant propagation distance of the beam in the chip substrate. It also determines the offset that has to be provided to shift the center of the microlens with respect to

Optics EXPRESS

Table 1. A list of the values of the expanded beam diameter and required radius of curvature (ROC) of the microlens to achieve beam collimation corresponding to different thicknesses of the silicon chip substrate. Starting beam waist = 4.6 μm (diameter = 9.2 μm), θ_{Si} = 4.06°, λ = 1310 nm.

Si Substrate Thickness (μm)	Expanded Beam Diameter (μm)	Radius of Curvature (μm)
200	13.4	205
300	16.9	245
400	21.7	310
500	26.2	370
600	31.0	440
700	36.3	515

the coupling position of the grating and hence, ensure that the beam is incident in an appropriate region of the microlens. As an example, for a grating coupler diffracting at 10° angle in oxide, the corresponding beam angle in silicon is 4.06°.

(iv) Lens offset from the optimum coupling position of the grating, O_L: Since the beam diffracted from the grating is directed at a certain angle θ_{Si} into the substrate, the center of the microlens has to be shifted by an offset O_L to ensure that the expanded optical beam hits an appropriate region of the microlens and gets collimated in the direction of the fiber. An improper placement of the microlens with respect to the grating might lead to a shift in the exit angle of the beam from the microlens, which would impact the coupling efficiency and/or a shift in the coupling spectrum (with the assumption that the position of the single-mode fiber or optical readout is fixed). As shown earlier in Fig. 1, the angular tolerance of the expanded beam reduces as the beam diameter increases. Thus, the larger the target beam diameter for an application, the more critical the lens offset parameter will be.

(v) Radius of curvature of the microlens, R_L: While the parameters (i)-(iii) determine the extent of the expansion of the beam, the collimation of the beam is achieved by calculating a specific radius of curvature of the microlens. A positive deviation of this value results in a divergent beam which is not fruitful to obtain a large longitudinal and lateral alignment tolerance from the interface. On the other hand, a negative deviation of this value results in a convergent beam that can perhaps be used to design an interface with a large working distance between the fiber and the microlens (with a limitation of requiring longer propagation distance between the grating and the microlens, and therefore, a thicker substrate). Considering the same conditions as mentioned in (ii), the corresponding values of R_L for different substrate thickness have been listed in Table 1. These values have been obtained from the Gaussian beam propagation method using a model designed in OpticStudio (Zemax) [37,44]. Since the microlens is spherical here, the beam angle, applied offset, and the calculated ROC are valid under the assumption of principal rays being orthogonal to the surface of the microlens.

(vi) Fiber mode-field diameter, W_{fiber}: The expanded collimated beam from the microlens placed at the chip backside is coupled to either an expanded beam interface such as a fiber array with integrated microlenses or a fiber with an expanded mode-field diameter as depicted in Fig. 2. Thus, the mode-field diameter of the out-coupling interface, W_{fiber}, is one of the target metrics that governs the parameters (i)-(iii).

All of these parameters hold key value in reaching the target of increased coupling tolerance to lateral and longitudinal misalignment. In the following sections in this paper, the system-level design is discussed for a specific case in O-band, but it should be noted that the generic design principles described in this section can also be applied for a different wavelength band (e.g. C-band), provided the grating design, beam diameter, beam divergence, chip substrate thickness, chip backside AR coating and microlens parameters are adjusted accordingly.

Optics EXPRESS

3. System-level optical design

The generic design principles described in the previous section were applied to a specific case of a photonics chip consisting of grating couplers operating around 1310 nm wavelength and a desired collimated beam diameter of 32 μm (beam diameter being dictated by the commercially available TEC fibers used for characterization). With these boundary conditions fixed, the thickness of the chip substrate was determined to be 600 μm, which resulted in a target ROC of 440 μm for the microlens. Also, the microlens was placed at an offset of 43 μm with respect to the coupling position of the uniformly periodic grating coupler (Fig. 3). This offset was computed by taking into account a 4.06° grating diffraction angle in silicon (600 μm $\times$ tan4.06°). Although grating couplers with metal reflectors deposited on top oxide provide high directionality towards the direction of the substrate [45,46], the experiment was performed on photonics dies consisting of regular grating couplers (Λ = 490 nm, fill-factor = 0.5) without the metal reflectors to facilitate fiber-coupling tests from both sides of the chip, and hence, provide ease in evaluation of various contributing factors of losses incurred in the expanded beam interface, as detailed in Section 5

The design schematic shown in Fig. 3(a) was directly implemented in Zemax OpticStudio and has been described in our previous work [37]. From the Zemax model, a sensitivity analysis of the coupling efficiency was carried out by varying the radius of curvature (ROC) of the microlens. Figure 4 shows the effect of variability of the ROC of the microlens on the resultant beam diameter and relative coupling efficiency to an expanded core fiber placed 100 μm distance away from the vertex of the microlens. The variation in beam diameter would occur due to the converging or diverging nature of the beam for a non-ideal value of ROC of the microlens, and results in a drop in the coupling efficiency. It was found that for a 1-dB tolerance in coupling efficiency to an expanded core fiber, a -100 μm and $+180$ μm variation in the ROC of the microlens is allowed. Although such numbers indicate a large tolerance of the ROC on fiber coupling efficiency at a given distance from the microlens, it should be noted that the beam collimation is affected as the ROC of the microlens deviates from an ideal value, which reduces the longitudinal alignment tolerance.

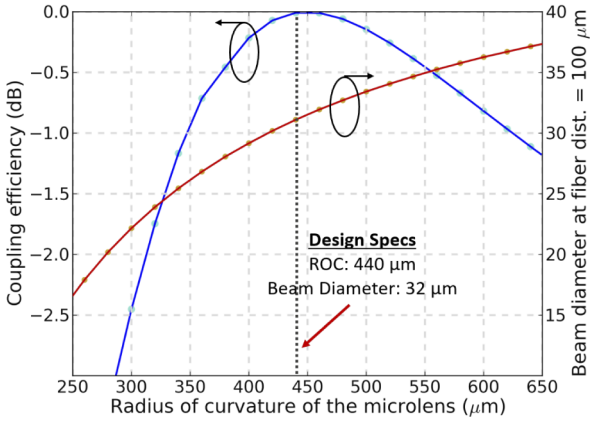

Fig. 4. For a 1-dB tolerance in coupling efficiency to an expanded core fiber, a -100 μm and $+180$ μm variation in the radius of curvature of the microlens was obtained.

4. Fabrication process flow

The fabrication of microlenses in silicon using resist reflow and reactive ion etching (RIE) has been widely investigated over several years and is a fairly mature technology now [47,48]. For the fabrication of silicon microlenses directly at the backside of the photonics chip, it was necessary

Optics EXPRESS

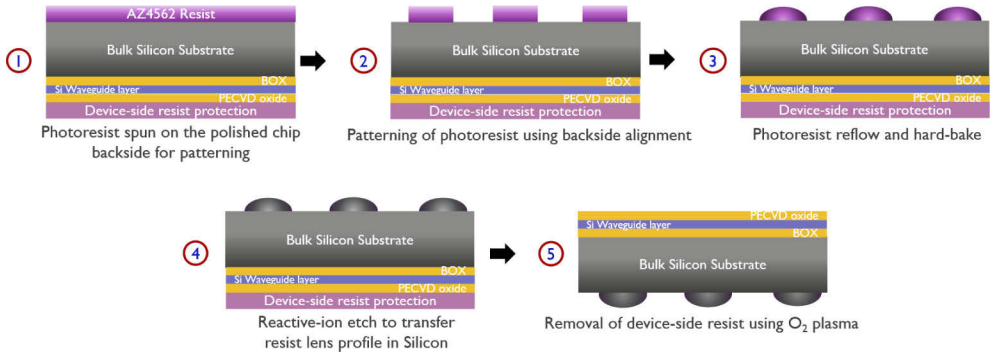

Fig. 5. Process flow for the fabrication of Si microlenses at the photonics chip backside.

that not only the microlenses were aligned and etched optimally with respect to the grating structures on the chip frontside, but also the SOI chip was backside polished and protected well from the front-side during processing. The process flow that was followed is illustrated in Fig. 5. Firstly, the photonics chip substrate was thinned and polished from the backside to a thickness of 600 μm [49]. The chip thickness was well-controlled in the central region where the lenses were fabricated in a later stage, the variation being ± 1 μm when introducing intermediate thickness measurements during thinning. The rms surface roughness obtained after polishing the chip is between 10-15 nm measured on an area of 1×1 cm^2. This is lower than $(\lambda/n_{Si})/20$ and can therefore be considered as an optically smooth surface. To begin processing on the backside of the photonics die for the fabrication of microlenses, the frontside of the die was protected by a photoresist layer. With the frontside of the die protected, the polished backside was spin coated with Microchem AZ4562 resist. To fabricate the lenses with a desired ROC (440 μm) in silicon, it is important that the resist thickness after spinning is well-controlled [50]. The target thickness of the resist here was 11.5 μm. The lithographic patterning of the microlens structures was performed using a dual-sided EVG mask aligner. This step is very critical, to ensure a backside-to-frontside alignment accuracy below ± 1 μm. After the patterns were exposed, and the exposed resist was removed during a developing step, the obtained cylindrical structures were reflowed at 145°C and hard-baked in an oven at 120°C. Thereafter, photoresist microlenses were transferred into silicon by an optimized reactive ion etch (RIE) process employing a mixture of SF_6 and O_2. The resist protection on the frontside of the photonics chip was removed later with the help of an O_2 plasma.

After fabrication, the microlenses were characterized using a white-light optical profilometer, and an ROC of 420 μm was obtained that was less than the target value by only 4.5% (Fig. 6). Also, an rms roughness of less than 10 nm was measured over the central region of the microlens spanning an area of 40×40 μm^2. Furthermore, the backside alignment accuracy after step 2, was estimated by inspecting the sample under a near IR-enabled diascopic illumination mode of the microscope. This enabled a through-substrate view of the photonics chip, viewed from the backside of the die. The microlenses were fitted with a circle and reference structures at the front side of the die were measured with respect to the fitted circle, as shown in Fig. 7(b). On comparing the measurements with those from the GDS design file (Fig. 7(a)), a difference in alignment of within ± 1 μm was obtained along both the directions of the grating. This indicates an actual alignment accuracy close to ± 1 μm, although the accuracy of the applied measurement method is not exactly known. To avoid any ambiguity, it must be noted that Fig. 6(a) depicts the testsite of grating-to-grating link with microlenses in resist and is shown here for illustration purposes.

Optics EXPRESS

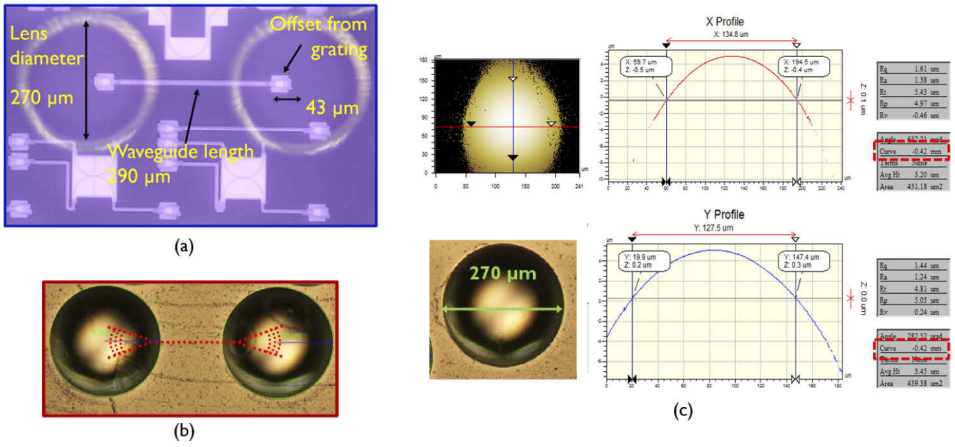

Fig. 6. (a) Diascopic near-IR view of the microlenses formed in resist; (b) Microscope image of the etched microlens; (c) A surface profilometer scan of microlens post-etch to determine the resulting diameter, sag and radius of curvature of the silicon microlens.

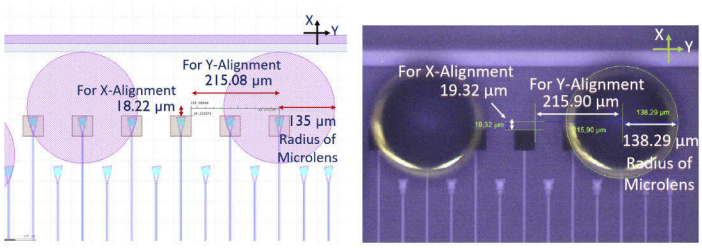

Fig. 7. (a) GDS design location of the grating structures with respect to the designed microlenses and (b) Diascopic (transmitted) NIR illuminated image from the microscope of the same design location. On comparing the markers with those from the GDS design file, a difference in microlens alignment of within ±1 μm was obtained along both the directions of the grating coupler.

5. Experiment and results

Since the chip consisted of regular uniformly periodic grating couplers and metal reflectors were not deposited above the grating, both the topside and the backside fiber coupling options were available. While a standard single-mode fiber (SMF28, MFD - 9.2 μm, NA - 0.14) was used to perform coupling from the topside of the chip, a thermally expanded core single-mode fiber (MFD - 32±2 μm, NA - 0.02) was used to couple the beam from the chip backside using microlens. Firstly, SMF28 fibers were used to couple in and out of the input and the output gratings from the device-side (topside) of the chip. Then, keeping the input fiber alignment with the grating intact, the optical beam exiting the microlens is coupled (from the backside of the chip) into a thermally expanded core fiber (TEC40) (Fig. 8). In this configuration, both the lateral and the angular alignment of the TEC40 fiber could be performed against the microlens fabricated with respect to the output grating, and a single microlens-to-fiber collimation property could be assessed. After the optimization of the backside fiber alignment with respect to the output microlens, the fiber input was shifted from the frontside to the backside of the die. The input fiber was also changed from SMF28 to TEC40 and aligned actively with respect to the microlens fabricated with respect to the input grating. Thus, an expanded mode coupling could

Optics EXPRESS

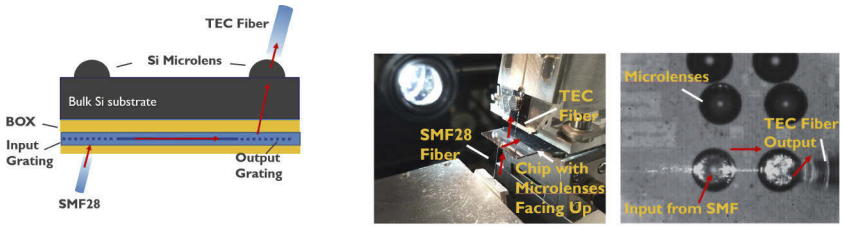

(a) (b) (c)

Fig. 8. Measurement methodology to align one TEC fiber with the microlens: The input fiber (SMF28) was used to launch the optical beam into the grating from the front-side of the die. The uniformly periodic output grating diffracts a part of the guided waveguide mode into the substrate that is coupled to the thermally expanded core fiber (TEC40) from the chip backside using the fabricated microlenses.

be performed from both the ends of the grating to evaluate the combined performance of the input and the output fiber-microlens system.

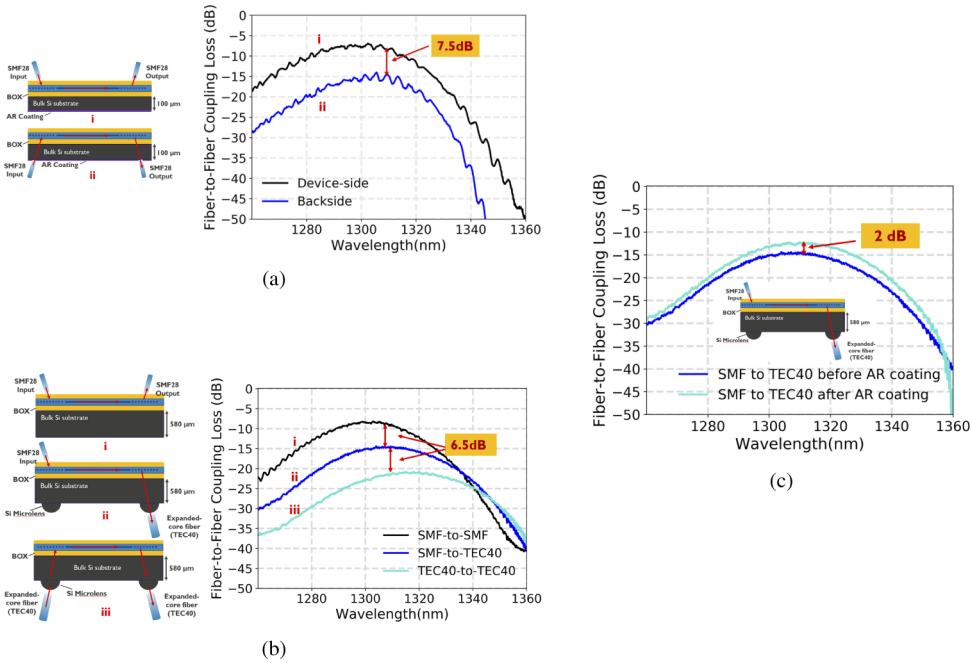

Fig. 9. (a) A comparison of (i) frontside vs. (ii) backside fiber-to-fiber coupling loss has been made for regular O-band grating couplers with a 490 nm period and 0.5 fill-factor; (b) The efficiency of the expanded beam interface was evaluated by comparing three measurements: (i) frontside SMF-to-SMF coupling loss, (ii) SMF (frontside)-to-TEC40 (backside) coupling loss and (iii) TEC40 (backside)-to-TEC40 (backside) coupling loss. Comparing graphs 9a.(ii) and 9b.(iii) results in an additional penalty of 3 dB due to increase in substrate thickness, the microlens, and the absence of AR coating; (c) An improvement of 2 dB in coupling efficiency was measured after the deposition of anti-reflection coating on the backside microlenses.

Since regular grating couplers were used to perform this experiment, firstly, a frontside versus backside coupling efficiency was measured using standard single-mode fibers (SMF28) on a

Optics EXPRESS

different chip with a substrate thickness of 100 μm, polished and AR-coated from the backside. This measurement provided a good reference to compare against the subsequent backside coupling measurements and thereby, deduce the coupling loss from a single expanded beam interface. Also, it is to be noted that the microlens and the grating coupler on either side of input/output is a combined entity, due to which the effect of each on the coupling efficiency cannot be separated out based on the current measurements. However, based on comparisons between different fiber-to-fiber coupling configurations and chip substrate thicknesses, the contribution of the combined grating-microlens entity to the loss can be derived and a projection can be made for further reduction of the loss when employing improved grating designs. As shown in Fig. 9(a) (depicting fiber-to-fiber coupling loss), an additional 3.75 dB loss per fiber-to-grating coupler interface occurs on shifting the fiber from the frontside (graph 9(a.i)) to the backside (graph 9(a.ii)) of the chip (with a lower net downward directionality due to Fresnel reflections from the BOX-silicon interface). Next, for the chip with the microlenses fabricated at its backside, the measured spectrum for SMF28 (frontside)-to-TEC40 (backside) and TEC40 (backside)-to-TEC40 (backside) configurations are shown via graphs 9(b.ii) and 9(b.iii) respectively in Fig. 9(b). The red shift of the center wavelength in graphs 9(b.ii) and 9(b.iii) is likely an outcome of using a thick substrate for beam expansion and the slope of absorption coefficient in bulk Si in O-band [51]. On comparing the graph 9(a.ii) and graph 9(b.iii), a difference of 6 dB in fiber-to-fiber backside coupling loss is obtained i.e. a 3 dB coupling loss is introduced in a single expanded beam interface due to the increase in substrate thickness, the microlens itself and the absence of AR coating on the microlens.

Table 2. Optical Loss Contribution In An Expanded Beam Interface

Measured Parameters		Loss
Backside coupling loss of a uniform grating (100 μm chip substrate thickness) - Fig. 9(a.ii)		7.5 dB
Improvement margin in coupling loss of expanded beam interface after the application of AR coating - Fig. 9(c)		2 dB
Coupling loss in a single grating-microlens expanded-beam interface (580 μm chip substrate thickness) - Fig. 9(b.iii) & Fig. 9(c)		8.5 dB
Projected coupling loss in a grating-microlens single expanded-beam interface employing gratings with metal reflectors and grating-to-microlens placement accuracy < ±0.5 μm	uniform	< 2.8 dB
	apodized	< 2 dB

Out of this additional 3 dB coupling loss, a 1.85 dB loss contribution was expected due to the Fresnel reflections from the silicon-air interface. This can be corrected by depositing an antireflective coating on the microlenses. To address this point, measurements were performed again on a single expanded beam interface after the deposition of 170 nm thick SiN anti-reflective (AR) coating. As can be seen via Fig. 9(c), an improvement of 2 dB was measured in the fiber (SMF)-to-fiber (TEC40) coupling efficiency. Also, no impact on the resultant bandwidth of the optical output was observed. A slightly higher improvement in coupling efficiency than the expected value indicates higher reflection of the beam that hits off-normal to the surface of the microlens, when the AR coating is not present. The cause of the remaining 1 dB loss from a single expanded beam interface can probably be attributed to the mode-profile mismatch due to the exponentially decaying field profile from the grating. Also, from the backside alignment analysis of microlens with respect to the grating that was reported earlier [37], a 0.5 dB coupling penalty can occur even if the fabricated microlenses are misplaced by ±1-1.5 μm from the desired location with respect to the grating. The applied offset of the microlens with respect to the grating coupler could also be improved after conducting a detailed design of experiment (DOE) during wafer-scale fabrication that can also account for the variability in beam angle from the grating at the intended wavelength of operation and radius of curvature of the microlens (Fig. 4). Thus, the

Optics EXPRESS

expanded beam coupling interface contributes to an additional 0.5-1 dB loss to the fiber-to-fiber link budget, implying that majority of the losses are incurred from the grating coupler itself.

It should be noted, as mentioned before, this paper is focused on realizing a monolithic expanded beam interface, and not to obtain the lowest possible total fiber-to-fiber loss. By decoupling the different losses, it is evident that minimizing the losses from the grating coupler will reduce the overall coupling penalty. This can be achieved by depositing metal reflectors above the grating couplers to improve the directionality and thereby, the overall fiber-to-fiber coupling performance, as has been reported via a hybrid integration experiment earlier (regular grating backside coupling efficiency used here being −7.5 dB in comparison to coupling efficiency of a backside grating with metal reflector being −2.3 dB) [37,45]. Thus, by improving the grating-to-microlens alignment accuracy to ±0.5 μm [37], and employing uniform gratings with metal reflectors, a single expanded beam interface incurring a 8.5 dB loss in this demonstration can be optimized further to lower the loss to 2.8 dB (8.5 - (7.5-2.3)- 0.5 = 2.8) or less. Moreover, if apodized gratings with metal reflectors are used (fiber-to-grating coupling efficiency ~ −1.5 dB [46]), the coupling loss of the expanded beam interface can be lowered down further to < 2 dB (8.5 - (7.5-1.5)−0.5 = 2), as projected in Table 2.

To assess the fiber-to-microlens alignment tolerance, an active alignment scan of the expanded core fiber was performed with respect to the microlenses at the backside of the chip. A ±7 μm and a ±9 μm 1-dB lateral alignment tolerance of the expanded core fiber was measured with respect to the longitudinal (X) and transverse (Y) axes of the grating coupler (Fig. 10(a)). This slight difference was expected because of the asymmetric size of the beam diffracted by the grating

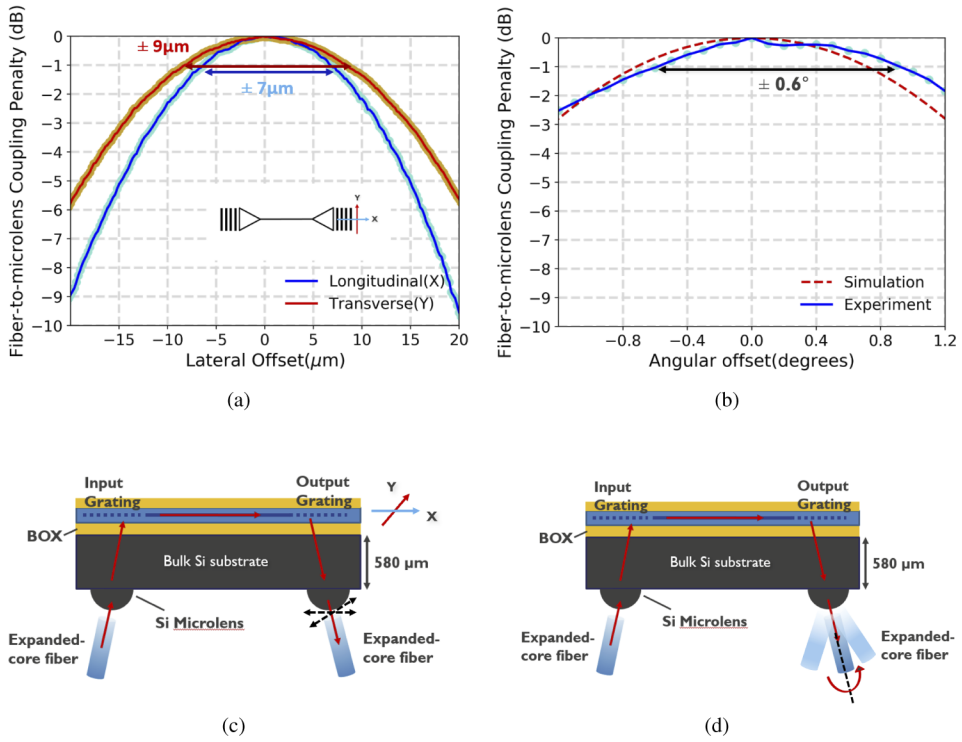

Fig. 10. (a,c) A ±7 μm and ±9 μm 1-dB alignment tolerance with respect to the longitudinal (X) and transverse (Y) axes of the grating and (b,d) ±0.6° angular 1-dB alignment tolerance was measured between an expanded mode coupled from the microlens to a single-mode expanded-core fiber.

Optics EXPRESS

coupler in both of the orthogonal directions [52]. Also, a ±0.6° angular 1-dB alignment tolerance was measured between the microlens and the expanded core fiber (Fig. 10(b)). These values are similar to those reported earlier by us in the hybrid integration experiment using microlenses at the backside of the photonics chip with a similar thickness of the silicon substrate [36].

Lastly, on retracting the expanded core fiber away from the microlens vertex successively in steps of 100 μm along the axis of the output beam, the fiber-to-microlens coupling efficiency was recorded at a fixed wavelength of 1310 nm. Fig. 11 shows that a 0.2 dB drop in the coupling efficiency was measured over a distance of 300 μm, when either of the input or the output fiber was retracted away from the microlens. Also, when both of the fibers were retracted together, a 1-dB coupling penalty occurs for a microlens-to-fiber separation of 400 μm. This is an outcome of the collimated nature of the beam, and also indicative of a large tolerance available in the longitudinal direction for an expanded beam connection.

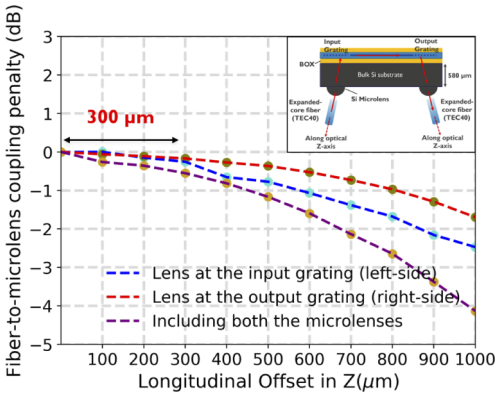

Fig. 11. On retracting the fibers individually along the axis of propagation of the collimated beam, a 0.2 dB drop in the coupling efficiency was measured over a distance of 300 μm. When both the fibers were retracted together, a 400 μm 1-dB longitudinal alignment tolerance was measured.

6. Discussion

It should be noted that the commercial availability and wide choice of mode field diameters of TEC fibers helped us to demonstrate the concept using these fibers. Clearly, these fibers can be replaced by a single-mode fiber ribbon mounted with a microlens array block, and can be used in the future to implement the presented concept. As can be noticed from the demonstrated results, the size of the microlens seems to be a limiting factor for applications addressing high on-chip and off-chip wiring density. In such a scenario, if fiber-ribbon arrays of 127 or 250 μm fiber pitch are used, lenses with low clear aperture would need to be fabricated to accommodate the high on-chip wiring density. It is to be noted that a lens of 270 μm diameter has been fabricated in our demonstration, and this value can be shrunk further by modifying the lens height to lens diameter ratio without changing the radius of curvature, if needed [53]. Moreover, if further increase in wiring density (and hence, lens diameter and pitch reduction) is required, other methods such as grayscale lithography, imprinting, direct writing based on 2-photon polymerization could be used. The design trade-off in that case would be to limit the beam expansion and hence, obtain a limited gain in the lateral alignment tolerance.

Although fibers have been used to demonstrate the concept of expanded beam coupling, the coupling to the microlens can be provided directly via a laser or VCSEL for specific applications. In that case a suitable microlens can be used to ensure that the laser/VCSEL emits a collimated beam with the desired diameter. A potential challenge will be to additionally provide the electrical

Optics EXPRESS

connections and to keep the form-factor of the entire module compact, and tackle the associated integration and assembly-level issues. This will depend on the type of laser. For a VCSEL, which is surface emitting, this seems very feasible, since a microlens can directly be mounted on top of the emitter, while for an edge-emitting laser, a mirror would have to be integrated to rotate the beam by 90 degrees to couple it to the microlens.

The key advantage of integrating the microlenses at the backside of the photonics chip is an increased tolerance to the lateral misalignment. Clearly, this is obtained at the expense of a reduced tolerance to angular misalignment in the coupling interface. The angular tilts, however, can be compensated or controlled more easily during assembly compared to lateral misalignments. Studies have already indicated a chip angular alignment accuracy of $\pm 0.1^\circ$, with a potential to achieve further improvement in passive assembly [29]. Thus, the demonstration of monolithically fabricated coupling interface is an attractive proposition to perform alignment-tolerant coupling in sensing applications or chip-to-board coupling for the face-up integration of a silicon photonics interposer.

7. Conclusion

We have reported results for monolithic integration of microlenses directly at the backside of a silicon photonics chip with a goal to achieve alignment-tolerant expanded beam interface. The design choices, fabrication process flow, and fiber coupling and alignment methodology were described comprehensively. A detailed investigation of the coupling performance and fiber-to-microlens alignment tolerance was carried out to underline the advantages of a SOI integrated photonics chip based expanded beam coupler. In particular, the expanded beam coupling interface adds a very small additional loss (0.5-1 dB) to the overall budget, with majority of the losses incurred from the grating coupler itself. By employing gratings with metal reflectors and $< \pm 0.5$ μm microlens-to-grating placement accuracy, losses under 2 dB have been projected for a monolithically integrated grating-microlens expanded beam interface. With an expanded beam diameter of 32 μm, a ± 7 μm lateral and a $\pm 0.6^\circ$ angular fiber-to-microlens 1-dB alignment tolerance was obtained at the wavelength of 1310 nm. Also, a large 300 μm longitudinal alignment tolerance with a 0.2 dB drop in coupling efficiency was obtained when the coupling was performed into a thermally expanded core (TEC) single-mode fiber. These relaxed alignment tolerance values are possible to obtain with wafer-scale backside integrated microlenses and can pave the way to perform coupling to a fiber array with a longer working distance or provide high-density on-board optical solution in the near future.

Acknowledgments. The primary author would like to thank the entire SiPh integration team at imec for providing help with the silicon photonics dies fabricated from 200-mm wafer-scale processing. Acknowledgments are also extended to Filip Vermeiren and Stijn Duynslager, CMST, Ghent University for their help with reactive-ion etching of microlenses and die-lapping respectively and Photonics Research Group (INTEC Department), Ghent University for help with SiN deposition. This work has been carried out as part of imec's industry affiliation program on Optical I/O, and the AQUARIUS project. The AQUARIUS project has received funding from the European Union's Horizon 2020 research and innovation programme under grant agreement No. 731465. This project is an initiative of the Photonics Public Private Partnership.

Disclosures. The authors declare that there are no conflicts of interest related to this article.

References

1. X. Chen, M. M. Milosevic, S. Stanković, S. Reynolds, T. D. Bucio, K. Li, D. J. Thomson, F. Gardes, and G. T. Reed, "The emergence of silicon photonics as a flexible technology platform," Proc. IEEE **106**(12), 2101–2116 (2018).
2. A. Rahim, T. Spuesens, R. Baets, and W. Bogaerts, "Open-access silicon photonics: current status and emerging initiatives," Proc. IEEE **106**(12), 2313–2330 (2018).
3. M. Binda, A. Canciamilla, A. Daverio, A. Fincato, P. Gambini, L. Maggi, P. Orlandi, L. Ramini, M. Repossi, A. Simbula, and M. Shaw, "High capacity silicon photonics packaging," in *2019 22nd European Microelectronics and Packaging Conference & Exhibition (EMPC)*, (IEEE, 2019), pp. 1–8.
4. A. Mekis, T. Pinguet, G. Masini, S. Sahni, M. Mack, S. Gloeckner, and P. De Dobbelaere, "Advanced silicon photonics transceivers," in *Silicon Photonics III*, (Springer, 2016), pp. 349–374.

Optics EXPRESS

5. H. Yu, J. Doylend, W. Lin, K. Nguyen, W. Liu, D. Gold, A. Dahal, C. Jan, R. Herrick, G. A. Ghiurcan, S. R. Hollingsworth, R. T. Romero, M. E. Favaro, L. Qiu, D. Zhu, and Y. Akulova, "100gbps cwdm4 silicon photonics transmitter for 5g applications,", in *Optical Fiber Communication Conference*, (Optical Society of America, 2019), pp. W3E–4.
6. M. J. Heck, "Highly integrated optical phased arrays: photonic integrated circuits for optical beam shaping and beam steering," Nanophotonics **6**(1), 93–107 (2017).
7. C. V. Poulton, A. Yaacobi, D. B. Cole, M. J. Byrd, M. Raval, D. Vermeulen, and M. R. Watts, "Coherent solid-state lidar with silicon photonic optical phased arrays," Opt. Lett. **42**(20), 4091–4094 (2017).
8. I. Staude and J. Schilling, "Metamaterial-inspired silicon nanophotonics," Nat. Photonics **11**(5), 274–284 (2017).
9. M. Khorasaninejad and F. Capasso, "Metalenses: Versatile multifunctional photonic components," Science **358**(6367), eaam8100 (2017).
10. S. A. Miller, M. Yu, X. Ji, A. G. Griffith, J. Cardenas, A. L. Gaeta, and M. Lipson, "Low-loss silicon platform for broadband mid-infrared photonics," Optica **4**(7), 707–712 (2017).
11. J.-M. Fedeli and S. Nicoletti, "Mid-infrared (mid-ir) silicon-based photonics," Proc. IEEE **106**(12), 2302–2312 (2018).
12. L. R. Chen, "Silicon photonics for microwave photonics applications," J. Lightwave Technol. **35**(4), 824–835 (2017).
13. J. S. Fandiño, P. Muñoz, D. Doménech, and J. Capmany, "A monolithic integrated photonic microwave filter," Nat. Photonics **11**(2), 124–129 (2017).
14. D. J. Moss, R. Morandotti, A. L. Gaeta, and M. Lipson, "New cmos-compatible platforms based on silicon nitride and hydex for nonlinear optics," Nat. Photonics **7**(8), 597–607 (2013).
15. M. Borghi, C. Castellan, S. Signorini, A. Trenti, and L. Pavesi, "Nonlinear silicon photonics," J. Opt. **19**(9), 093002 (2017).
16. J. W. Silverstone, J. Wang, D. Bonneau, P. Sibson, R. Santagati, C. Erven, J. O'Brien, and M. Thompson, "Silicon quantum photonics,", in *2016 International Conference on Optical MEMS and Nanophotonics (OMN)*, (IEEE, 2016), pp. 1–2.
17. T. Rudolph, "Why i am optimistic about the silicon-photonic route to quantum computing," APL Photonics **2**(3), 030901 (2017).
18. Y. Shen, N. C. Harris, S. Skirlo, M. Prabhu, T. Baehr-Jones, M. Hochberg, X. Sun, S. Zhao, H. Larochelle, D. Englund, and M. Soljačić, "Deep learning with coherent nanophotonic circuits," Nat. Photonics **11**(7), 441–446 (2017).
19. D. A. Miller, "Silicon photonics: Meshing optics with applications," Nat. Photonics **11**(7), 403–404 (2017).
20. Q. Cheng, J. Kwon, M. Glick, M. Bahadori, L. P. Carloni, and K. Bergman, "Silicon photonics codesign for deep learning," Proc. IEEE (2020).
21. A. N. Tait, T. F. De Lima, E. Zhou, A. X. Wu, M. A. Nahmias, B. J. Shastri, and P. R. Prucnal, "Neuromorphic photonic networks using silicon photonic weight banks," Sci. Rep. **7**(1), 7430 (2017).
22. A. Katumba, M. Freiberger, F. Laporte, A. Lugnan, S. Sackesyn, C. Ma, J. Dambre, and P. Bienstman, "Neuromorphic computing based on silicon photonics and reservoir computing," IEEE J. Sel. Top. Quantum Electron. **24**(6), 1–10 (2018).
23. R. Marchetti, C. Lacava, L. Carroll, K. Gradkowski, and P. Minzioni, "Coupling strategies for silicon photonics integrated chips," Photonics Res. **7**(2), 201–239 (2019).
24. B. W. Snyder, "Hybrid integration and packaging of grating-coupled silicon photonics," Ph.D. thesis, University College Cork (2013).
25. T. Barwicz, Y. Taira, T. W. Lichoulas, N. Boyer, Y. Martin, H. Numata, J.-W. Nah, S. Takenobu, A. Janta-Polczynski, E. L. Kimbrell, R. Leidy, M. W. Khater, S. Kamlapurkar, S. Engelmann, Y. A. Vlasov, and P. Fortier, "A novel approach to photonic packaging leveraging existing high-throughput microelectronic facilities," IEEE J. Sel. Top. Quantum Electron. **22**(6), 455–466 (2016).
26. G. B. Preve, "Problems, challenges, and a critical survey on automated silicon photonics packaging and optical interconnection," in *Optical Interconnects XIX*, vol. 10924 (International Society for Optics and Photonics, 2019), p. 1092415.
27. T. Barwicz, T. W. Lichoulas, Y. Taira, Y. Martin, S. Takenobu, A. Janta-Polczynski, H. Numata, E. L. Kimbrell, J.-W. Nah, B. Peng, D. Childers, R. Leidy, M. Khater, S. Kamlapurkar, E. Cyr, S. Engelmann, P. Fortier, and N. Boyer, "Breaking the mold of photonic packaging," in *Integrated Optics: Devices, Materials, and Technologies XXII*, vol. 10535 (International Society for Optics and Photonics, 2018), p. 105350R.
28. W. Joyce and B. DeLoach, "Alignment of gaussian beams," Appl. Opt. **23**(23), 4187–4196 (1984).
29. S. D. Le, P. Rochard, J.-B. Briand, L. Quétel, S. Claudot, and M. Thual, "Coupling efficiency and reflectance analysis of graded index expanded beam connectors," J. Lightwave Technol. **34**(9), 2092–2099 (2016).
30. T. Barwicz, N. Boyer, A. Janta-Polczynski, J.-F. Morissette, Y. Thibodeau, L. Patry, T. W. Lichoulas, E. L. Kimbrell, S. Martel, S. Kamlapurkar, S. Engelmann, R. L. Bruce, Y. A. Vlasov, and P. Fortier, "A metamaterial converter centered at 1490nm for interfacing standard fibers to nanophotonic waveguides," in *2016 Optical Fiber Communications Conference and Exhibition (OFC)*, (IEEE, 2016), pp. 1–3.
31. D. Benedikovic, C. Alonso-Ramos, P. Cheben, J. H. Schmid, S. Wang, R. Halir, A. Ortega-Moñnux, D.-X. Xu, L. Vivien, J. Lapointe, S. Janz, and M. Dado, "Single-etch subwavelength engineered fiber-chip grating couplers for 1.3 μm datacom wavelength band," Opt. Express **24**(12), 12893–12904 (2016).

Optics EXPRESS

32. S. Khan, S. M. Buckley, J. Chiles, R. P. Mirin, S. W. Nam, and J. M. Shainline, "Low-loss, high-bandwidth fiber-to-chip coupling using capped adiabatic tapered fibers," APL Photonics **5**(5), 056101 (2020).
33. P.-I. Dietrich, M. Blaicher, I. Reuter, M. Billah, T. Hoose, A. Hofmann, C. Caer, R. Dangel, B. Offrein, U. Troppenz, M. Moehrle, W. Freude, and C. Koos, "In situ 3D nanoprinting of free-form coupling elements for hybrid photonic integration," Nat. Photonics **12**(4), 241–247 (2018).
34. S. Thomas, K. Y. Bastardo, and M. K. Anselm, "Industry trends in photonics packaging: passive fiber and die coupling,", in *2017 Pan Pacific Microelectronics Symposium (Pan Pacific)*, (IEEE, 2017), pp. 1–8.
35. C. Scarcella, K. Gradkowski, L. Carroll, J.-S. Lee, M. Duperron, D. Fowler, and P. O'Brien, "Pluggable single-mode fiber-array-to-PIC coupling using micro-lenses," IEEE Photonics Technol. Lett. **29**(22), 1943–1946 (2017).
36. N. Mangal, J. Missinne, G. Roelkens, J. V. Campenhout, G. V. Steenberge, and B. Snyder, "Expanded-beam through-substrate coupling interface for alignment tolerant packaging of silicon photonics,", in *2018 Optical Fiber Communications Conference and Exposition (OFC)*, (IEEE, 2018), pp. 1–3.
37. N. Mangal, B. Snyder, J. Van Campenhout, G. Van Steenberge, and J. Missinne, "Expanded-beam backside coupling interface for alignment-tolerant packaging of silicon photonics," IEEE J. Sel. Top. Quantum Electron. **26**(2), 1–7 (2020).
38. J. Missinne, N. T. Benéitez, N. Mangal, J. Zhang, A. Vasiliev, J. Van Campenhout, B. Snyder, G. Roelkens, and G. Van Steenberge, "Alignment-tolerant interfacing of a photonic integrated circuit using back side etched silicon microlenses," in *Silicon Photonics XIV*, vol. 10923 (International Society for Optics and Photonics, 2019), p. 1092304.
39. N. Mangal, J. Missinne, J. Van Campenhout, G. Van Steenberge, and B. Snyder, "Through-substrate coupling elements for silicon-photonics-based short-reach optical interconnects," in *Optical Interconnects XIX*, vol. 10924 (International Society for Optics and Photonics, 2019), p. 109240D.
40. R. Meade, S. Ardalan, M. Davenport, J. Fini, C. Sun, M. Wade, A. Wright-Gladstein, and C. Zhang, "Teraphy: A high-density electronic-photonic chiplet for optical i/o from a multi-chip module,", in *2019 Optical Fiber Communications Conference and Exhibition (OFC)*, (IEEE, 2019), pp. 1–3.
41. N. Mangal, J. Missinne, J. Van Campenhout, B. Snyder, and G. Van Steenberge, "Ball lens embedded through-package via to enable backside coupling between silicon photonics interposer and board-level interconnects," J. Lightwave Technol. **38**(8), 2360–2369 (2020).
42. M. Kihara, M. Matsumoto, T. Haibara, and S. Tomita, "Characteristics of thermally expanded core fiber," J. Lightwave Technol. **14**(10), 2209–2214 (1996).
43. J. Nishimura and K. Morishita, "Mode-field expansion and reduction in dispersive fibers by local heat treatments," IEEE J. Sel. Top. Quantum Electron. **5**(5), 1260–1265 (1999).
44. Z. OpticStudio, "15.5," Zemax LLC, Seattle, WA (2016).
45. N. Mangal, J. Missinne, G. Van Steenberge, J. Van Campenhout, and B. Snyder, "Performance evaluation of backside emitting O-Band grating couplers for 100 μm-thick silicon photonics interposers," IEEE Photonics J. (2019).
46. N. Mangal, "Alignment-tolerant coupling interfaces for board-level integration of silicon photonics," Ph.D. thesis, Ghent University (2020).
47. P. Savander, "Microlens arrays etched into glass and silicon," Opt. Lasers Eng. **20**(2), 97–107 (1994).
48. M. Eisner and J. Schwider, "Transferring resist microlenses into silicon by reactive ion etching," Opt. Eng. **35**(10), 2979–2982 (1996).
49. E. Bosman, "Integration of optical interconnections and optoelectronic components in flexible substrates," Ph.D. thesis, Ghent University (2010).
50. D. Daly, R. Stevens, M. Hutley, and N. Davies, "The manufacture of microlenses by melting photoresist," Meas. Sci. Technol. **1**(8), 759–766 (1990).
51. M. A. Green, "Self-consistent optical parameters of intrinsic silicon at 300 k including temperature coefficients," Sol. Energy Mater. Sol. Cells **92**(11), 1305–1310 (2008).
52. D. Taillaert, "Grating couplers as interface between optical fibres and nanophotonic waveguides." Ph.D. thesis, Ghent University (2005).
53. P. Nussbaum, R. Voelkel, H. P. Herzig, M. Eisner, and S. Haselbeck, "Design, fabrication and testing of microlens arrays for sensors and microsystems," Pure Appl. Opt. **6**(6), 617–636 (1997).